ACS NANO

www.acsnano.org

ARTICLE

Nanoceria as an Electron Reservoir: Spontaneous Deposition of Metal Nanoparticles on Oxides and Their Anti-inflammatory Activities

Faheem Muhammad,[†] Futao Huang,[†] Yuan Cheng,[†] Xiwen Chen, Quan Wang, Chenxin Zhu, Yihong Zhang, Xiaohan Yang, Peng Wang, and Hui Wei*

Cite This: *ACS Nano* 2022, 16, 20567−20576

Read Online

ACCESS | Metrics & More | Article Recommendations | Supporting Information

ABSTRACT: **Designing metal−metal oxide heteronanostructures with synergistic and superior activities (unattainable in the case of a single entity) is of great interest for a wide range of technological applications. Traditional synthetic strategies typically require reducing agents, stabilizing ligands, or high temperature reductive treatment to produce oxide-supported metals. Herein, a facile noble metal deposition strategy is developed to produce silver, gold, and platinum nanocrystals on the surface of hollow mesoporous cerium oxide nanospheres without any pretreatment. Unlike the galvanic replacement reaction, the developed protocol employs the innate reductive potential of CeO_2 to produce a high density of ultrafine noble metal nanocrystals homogeneously immobilized onto the surface of CeO_2 nanospheres. The multienzyme-like activities (i.e., superoxide dismutase-like and catalase-like) of CeO_2@metal nanostructures, originating from CeO_2 and metal nanoparticles, were effectively utilized for anti-inflammatory therapies in two *in vivo* models. This oxygen vacancy-mediated reduction strategy can be generalized to produce diverse metal−metal oxide nanostructures for a wide range of applications.**

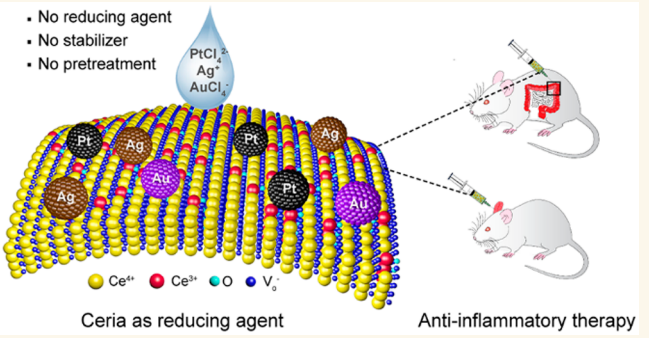

KEYWORDS: *Noble Metal Catalyst, Nanozyme, Nanoceria, Oxygen Vacancy, Reactive Oxygen Species, Anti-inflammatory Therapy*

INTRODUCTION

Noble metal nanostructures exhibit fascinating catalytic properties for a wide range of reactions important in the chemical and pharmaceutical industries, but the downside is that during the synthesis or under catalytic operating conditions, sintering or coalescence invariably deteriorates the quality of metal nanoparticles (NPs) because of the thermodynamically unstable nature.[1−5] Deposition of noble metal catalysts onto metal oxide supports has been proven to be one of the most effective strategies to stabilize the NPs. Supported NPs display improved activities compared to their nonsupported counterparts due to the synergetic effects originated at the metal−metal oxide heterojunction via altered electronic structures.[6−14] A range of precious metal catalysts have been so far loaded on different transition or nontransition metals oxides with the purpose of improving stability and attaining enhanced activity.[15−21] The incipient impregnation, chemical vapor deposition, laser ablation, and electrochemical deposition approaches have been adopted for deposition of metal NPs.[22−27] Alternatively, high-quality monodispersed metal NPs with a narrow particle size distribution are synthesized under the protection of stabilizers (i.e., polymer or surfactant) prior to loading on supports, but the presence of the stabilizers at the interface between the metal NPs and the support minimizes the direct contact or electronic communication between metals and supports.[28−31] Naked NPs with maximum active surface areas are mostly the desired product; there have been few reports where bare metal NPs were *in situ* grown outside or inside metal oxides structures.[32−34] For

Received: July 22, 2022
Accepted: November 14, 2022
Published: November 17, 2022

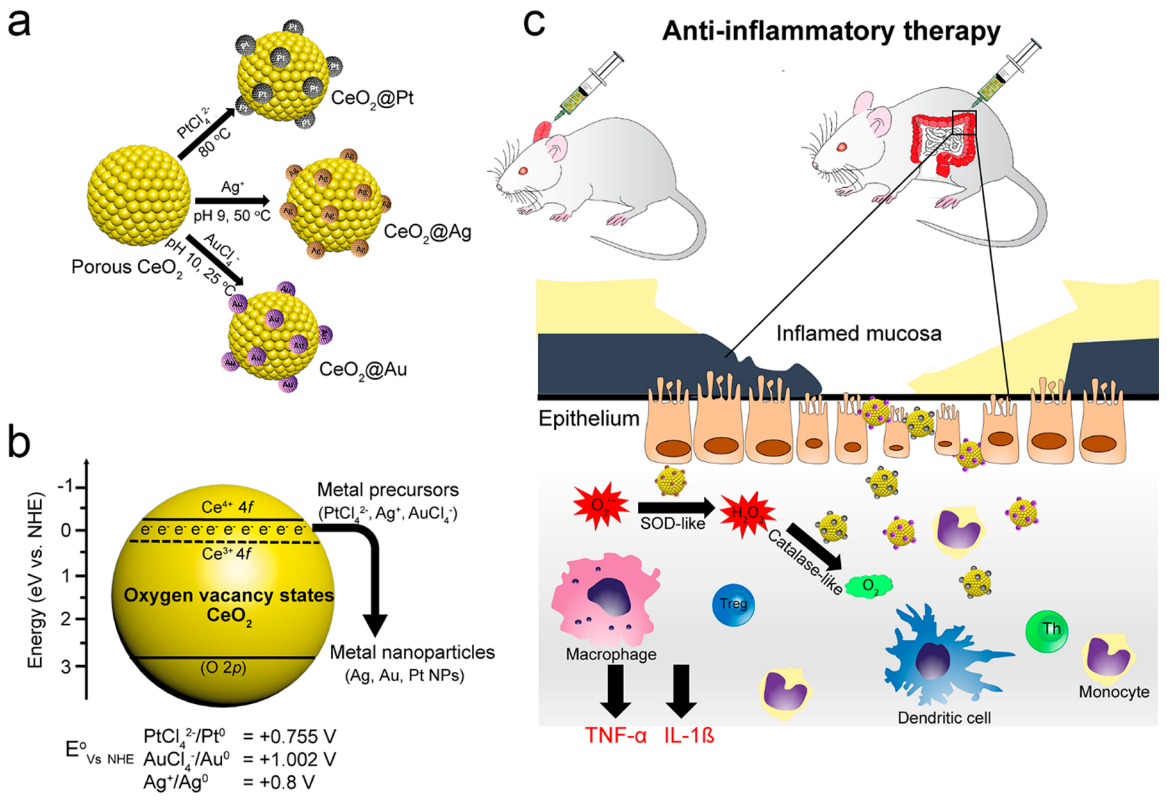

Figure 1. Synthesis of CeO_2@metal nanozymes and their application for inflammatory disease treatments. (a) Schematic diagram representing the synthetic protocol to spontaneously grow noble metal NPs onto the surface of hollow ceria nanospheres. (b) Scheme illustrating the oxygen vacancy-mediated appearance of energy states in mixed-valent nanoceria and the subsequent reduction of metal salts into metal NPs. (c) Schematic diagram showing the multiple enzyme-like activities of CeO_2@metal in treating IBD and ear inflammation.

instance, MnO nanocrystals were used as a reactive template to electrolessly deposit platinum NPs onto the surface via the galvanic replacement reaction.[35,36] In other reports, noble metal NPs were deposited on WO_2 nanowires and TiO_2 NPs.[37−39] There have been reports wherein metal core cerium oxide shelled based nanostructures were produced using wet chemical reaction systems.[40−43] In this study, we report as-synthesized hollow CeO_2 nanospheres as an electron reservoir to reduce the metal salts into metal NPs under optimized synthetic conditions, in contrast to previous reports wherein CeO_2 shells were formed on metal NPs. In this study, metal NPs were spontaneously deposited onto the surface of well-defined hollow CeO_2 nanospheres without using any additional pretreatments, reducing agents, or surfactants.

Functional nanomaterials with enzyme-like activities, called nanozymes, have recently received great attention, both nanoceria and noble metal NPs have individually demonstrated promising enzymatic activities.[44−51] Their enzyme-like activities have also been explored for treating reactive oxygen species (ROS)-linked ailments.[52−56] Keeping in view the therapeutic potential, we exploited the innate antioxidant characteristics of our CeO_2@metal nanostructures in inflammatory bowel disease (IBD) and ear inflammation models, our findings revealed an enhanced ROS scavenging capacities of CeO_2@metal nanozymes which subsequently halted the progression of inflammation via downregulation of the pro-inflammatory cytokines: interleukin-1 beta (IL-1β) and tumor necrosis factor-alpha (TNF-α). Among the three nanozymes, CeO_2@Ag displayed superior therapeutic activity, which was ascribed to its excellent superoxide dismutase (SOD)- and catalase (CAT)-like activities. The CeO_2@Ag with a concentration as low as 0.5 mg/kg body weight appreciably halted the inflammation process in both IBD and ear inflammation models.

RESULTS AND DISCUSSION

Nanoceria contains an appreciable amount of trivalent cerium (Ce^{3+}) and oxygen vacancies (OVs); the presence of such crystal structure with mixed oxidation states and defects motivated us to use nanoceria as a reducing agent for the spontaneous growth of noble metals. For a proof-of-concept study, we selected three kinds of CeO_2: ultrasmall NPs, self-assembled hollow nanospheres with higher concentrations of Ce^{3+} (33−35%), and nanorods (NRs) having lower Ce^{3+} content (19.34%). Considering the distinct standards redox potentials and physiochemical properties, the synthetic conditions were first optimized via changing the pH and temperature of the reaction solutions. Initially, a known amount of metal salts ($HAuCl_4$, $AgNO_3$, and K_2PtCl_4) was merely mixed with an aqueous solution of CeO_2 hollow nanospheres at room temperature without adjusting the pH and the reaction temperatures. No apparent change in the color of the solution was observed after 24 h, as shown in Figure S1a; however, tuning the pH resulted in a marked variation in the color of solutions, and spontaneous generation of metallic NPs on the CeO_2 surface was apparently visualized with the formation of colored products in case of NPs and hollow nanospheres (Figure S1b). Unlike the growth of Ag and Au NPs, synthesis of Pt required a higher temperature by virtue of a relatively low standard redox potential and physiochemical properties of the precursor salt. An obvious

https://doi.org/10.1021/acsnano.2c07306
ACS Nano 2022, 16, 20567−20576

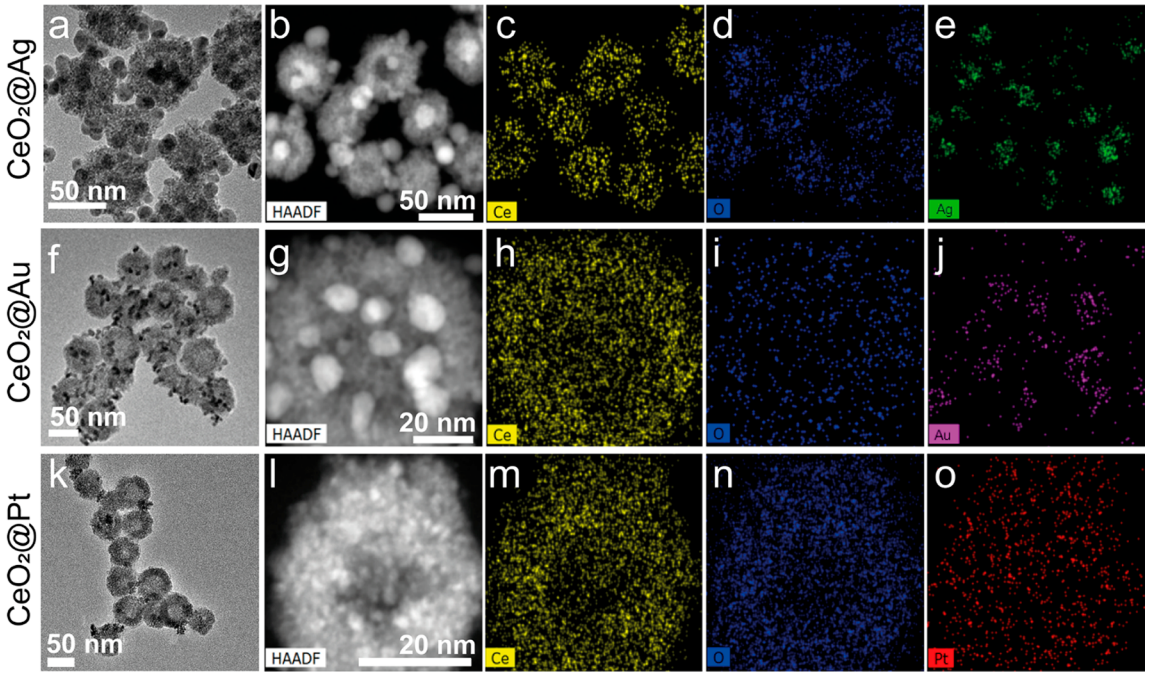

Figure 2. TEM images, HAADF-STEM images, and EDS elemental mappings indicate the growth of different noble metal NPs onto the surface of CeO_2 hollow nanospheres. (a–e) CeO_2@Ag, (f–j) CeO_2@Au, and (k–o) CeO_2@Pt nanostructures.

color change (blackish product) was observed when the temperature was raised to 80 °C (Figure S1c). The generation of metallic NPs was observed in the case of both NPs and hollow nanospheres. However, no metal NPs growth was observed in the case of CeO_2 NR under similar synthetic conditions, as witnessed by the absence of apparent color changes in solutions. The lower content of Ce^{3+} (OVs) in NRs implies the less availability of surface trapped electrons to reduce the metal precursors into metal NPs.

Mechanistically, the presence OVs causes the appearance of an intermediate energy level between the valence band (VB) and conduction band (CB) and electrons tend to accumulate around that defect-associated energy level.[37] If the reduction potential of the OVs is much lower than that of the metal salts, the relative potential differences drive the spontaneous electron transfer from the OVs to the metal ions, thus resulting in the generation of metallic NPs.[57,58] In our study, standard reduction potential values of metal precursors are positive: $AuCl_4^-$ (E^0 vs NHS = +1.002 V) was readily reduced at room temperature, while the Ag^+ (E^0 vs NHS = +0.8 V) reduction and NPs growth was observed at a moderately higher temperature. The transformation of $PtCl_4^{2-}$ (E^0 vs NHS = +0.755 V) and the resulting NPs required further higher temperatures (Figure 1b). Ultrasmall ceria NPs and ceria nanorods were prepared using our previous reported method, while the hollow CeO_2 nanospheres were synthesized via a polyol-mediated solvothermal approach in the presence of hydrochloric acid (HCl).[59] The size and morphology of different CeO_2 substrates and respective nanostructures were investigated by transmission electron microscopy (TEM). Figure S2a–e shows the ultrasmall CeO_2 and corresponding CeO_2@metal nanostructures: Ag and Au NPs could be easily observed in the images, while due to their very small size, Pt NPs were analyzed via scanning transmission electron microscopy (STEM). The morphology and composition of CeO_2 NRs is shown in Figure S3. Because of the inactive nature of NRs to reduce metal precursors and the relatively aggregated nature of ultrasmall CeO_2 NPs@metal, we confined our further study to the monodispersed and uniform hollow CeO_2 nanospheres. As can be seen in Figure S4, the size of hollow structured CeO_2 nanospheres is around 80 nm. High resolution (HR)TEM and STEM images reveal that the porous hollow nanospheres is actually composed of self-assembled smaller CeO_2 NPs (3–4 nm). Prior to redox reactions with metal precursors, the surface of CeO_2 nanospheres was smooth and clean, whereas distinct changes were observed following the metal precursors treatment, the obtained CeO_2@metal nanostructures are shown in Figure 2.

TEM images of CeO_2@Ag unambiguously show Ag NPs (5–10 nm) decorated onto CeO_2 nanospheres, the high angle annular dark field (HAADF)-STEM images indicate the presence and distribution of Ag and Ce elements in the nanospheres (Figure 2a–e). In the case of gold deposition, the HAADF-STEM image shows electron-dense NPs studded CeO_2 nanospheres. Unlike gold and silver, platinum growth, however, required a relatively higher temperature and the NPs were also smaller in size in the form of clusters (as depicted in Figure 2k). The appearance of both platinum and cerium signals (as shown as yellow and red colors in Figure 2) in CeO_2@Pt revealed the electroless deposition of platinum NPs. Before the electron transfer for reduction reaction, the adsorption of cationic/anionic metal precursors onto the surface of CeO_2 is a precondition. In view of this, we determined the zeta potential of CeO_2 substrates in the 2–11 pH range. Figure S5 shows the zeta potentials of all the three CeO_2 nanostructures and the values were found to be positive up to pH 8, probably due to the presence of high Ce^{3+} content and the naked surfaces of CeO_2 NPs and NRs, while the hollow CeO_2 nanospheres were stabilized by a neutral polymer (PVP). The positively charged surfaces of different CeO_2 nanostructures electrostatically attract the negatively charged metal precursors ($AuCl_4^-$, $PtCl_4^{2-}$), while at pH 9 and above,

https://doi.org/10.1021/acsnano.2c07306
ACS Nano 2022, 16, 20567–20576

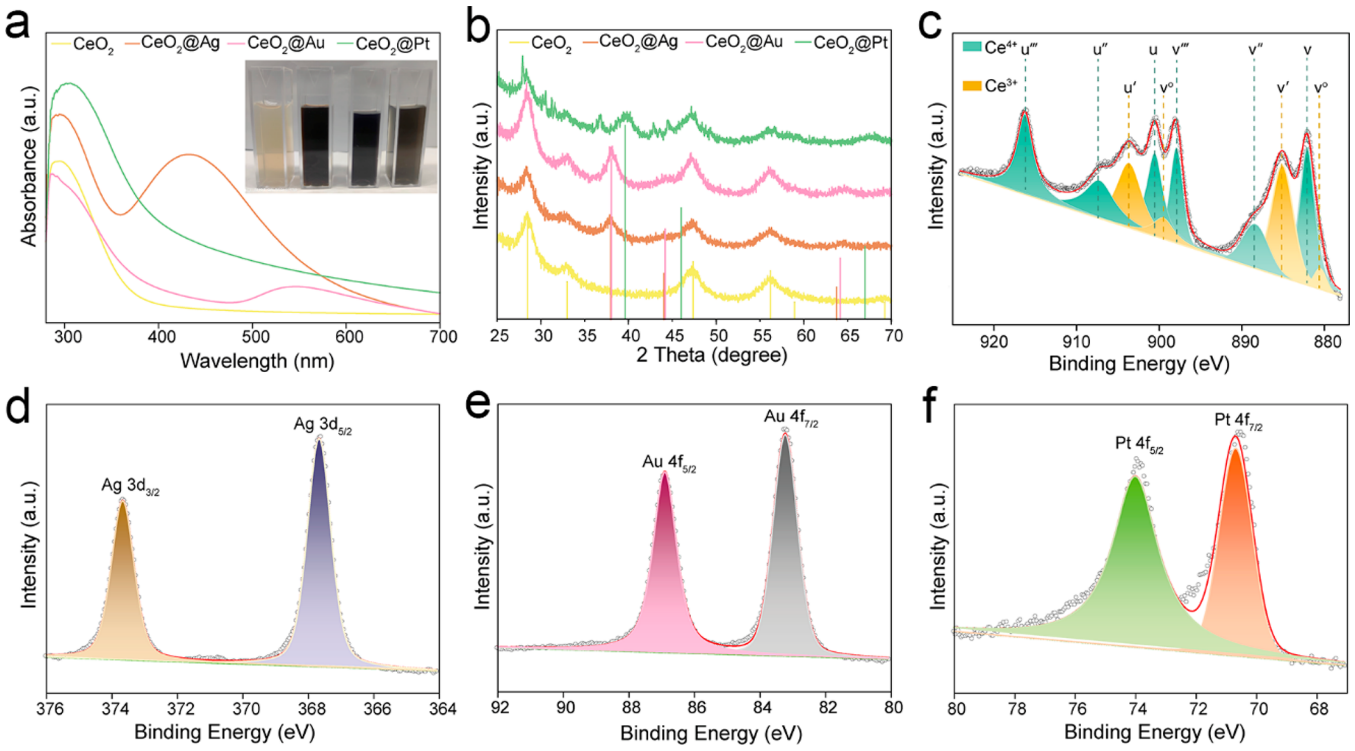

Figure 3. (a) Visible extinction spectra and corresponding digital images (inset, from left to right: CeO_2, CeO_2@Ag, CeO_2@Au, and CeO_2@Pt). (b) XRD patterns of CeO_2, CeO_2@Ag, CeO_2@Au, and CeO_2@Pt nanostructures. (c–f) X-ray photoelectron spectra (XPS) of different CeO_2@metal nanostructures: (c) Ce 3*d*, (d) Ag 3*d*, (e) Au 4*f*, and (f) Pt 4*f*.

the zeta potential values were negative and thus the *in situ* formed positively charged diamine silver complex $[Ag(NH_3)_2]^+$ could readily anchor onto CeO_2 surface. The variation in the zeta potential values and colors of the solution following metal precursors adsorption onto the surface CeO_2 nanostructures are shown in Figures S6–8. In addition to determining the zeta potentials following 1 min incubation of CeO_2 with metal precursors, the centrifuged and washed samples were also examined via STEM. Figure S9 verifies the fast adsorption of metal precursors and subsequent growth of well-defined Ag and Au NPs, the presence of very small Pt NPs and elemental mapping signals also corroborates the adsorption of $PtCl_4^{2-}$ salt on positively charged CeO_2 surface.

Being an effective analytical technique to monitor the growth of plasmonic-active metal NPs, the absorption spectra indicated the appearance of plasmonic peaks in both Ag and Au nanostructures (Figure 3a). The absorption peak at 435 nm was detected in a dark brown colored CeO_2@Ag solution, while a broad and weak absorption peak centered at ∼540 nm appeared in CeO_2@Au product. In the case of a black CeO_2@Pt solution, no absorption peak was expected to be observed in the visible region because Pt absorbs in the UV region (∼260 nm). Similarly, the optical properties of ultrasmall CeO_2 NPs based nanostructures also verified the growth of metal NPs (Figure S2f).

Powder X-ray diffraction (XRD) patterns indicate the crystal structure of pure CeO_2 with a cubic fluorite structure (JCPDS file no. 34-0394). In addition to CeO_2 peaks, the appearance of two prominent peaks at 38.1° and 44.09° corresponded to the (111) and (200) planes of silver in CeO_2@Ag. Similarly, the existence and crystalline nature of gold was verified via the observation of peaks at 38.33° and 44.86° (JCPDS file no. 04-0784). The XRD pattern of CeO_2@Pt showed a distinct peak at 39.90° indexed to the (111) plane, implying the presence of a face-centered cubic crystal lattice of platinum (JCPDS file no. 04-0802). Valence state and the composition of the nanostructures were characterized via X-ray photoelectron spectroscopy (XPS). As shown in Figure S10, the peaks of Ce 3*d*, Ag 3*d*, Pt 4*f*, Au 4*f*, O 1*s*, and C 1*s* were observed in the survey spectra. The mixed oxidation states of nanoceria were revealed in the Ce 3*d* spectrum when resolved into 10 different peaks (u^0, *u*, *u*′, *u*″, and *u*‴ for $3d_{3/2}$ and v^0, *v*, *v*′, *v*″, and *v*‴ for $3d_{5/2}$).[60,61] The content of trivalent state was found to be around 33.64% (Figure 3c), the existence of both Ce^{3+} and Ce^{4+} in CeO_2 and the resulting oxygen vacancy provides excess electrons (changes Ce^{4+} to Ce^{3+}) per vacancy, the availability of those excess electrons was exploited in this study to reduce metal precursors into a series of noble metal NPs. Following the reactions with metal salts, we quantified the changes in Ce^{3+} content and a noticeable reduction in the peaks and quantities of Ce^{3+} from 33.64% to ∼25.5% was observed in the cases of CeO_2@Ag and CeO_2@Au nanostructures (Figure S11). No obvious variation in Ce^{3+} content in CeO_2@Pt nanostructures might be due to electron transfer from metallic Pt into CeO_2 (a slight peak shift was also noticed). In the resolved spectrum of oxygen of CeO_2, two Gaussian peaks associated with lattice oxygen and the surface-bound oxygen from the vacancies or −OH groups were observed (Figure S12). The deposition of metallic silver was revealed by the appearance of characteristic peaks at 368.0 and 374.0 eV in the Ag 3*d* spectrum corresponding to the binding energies (BEs) of Ag $3d_{5/2}$ and Ag $3d_{3/2}$ of metallic Ag^0. Peaks at 84.0 and 88.0 eV were attributed to Au $4f_{7/2}$ and Au $4f_{5/2}$, respectively; the doublet with distinct binding energies of 70.5 (Pt $4f_{7/2}$) and 73.9 eV (Pt $4f_{5/2}$) corresponded to metallic Pt^0. We found CeO_2 NRs as an inactive substrate to produce metal NPs and

https://doi.org/10.1021/acsnano.2c07306
ACS Nano 2022, 16, 20567−20576

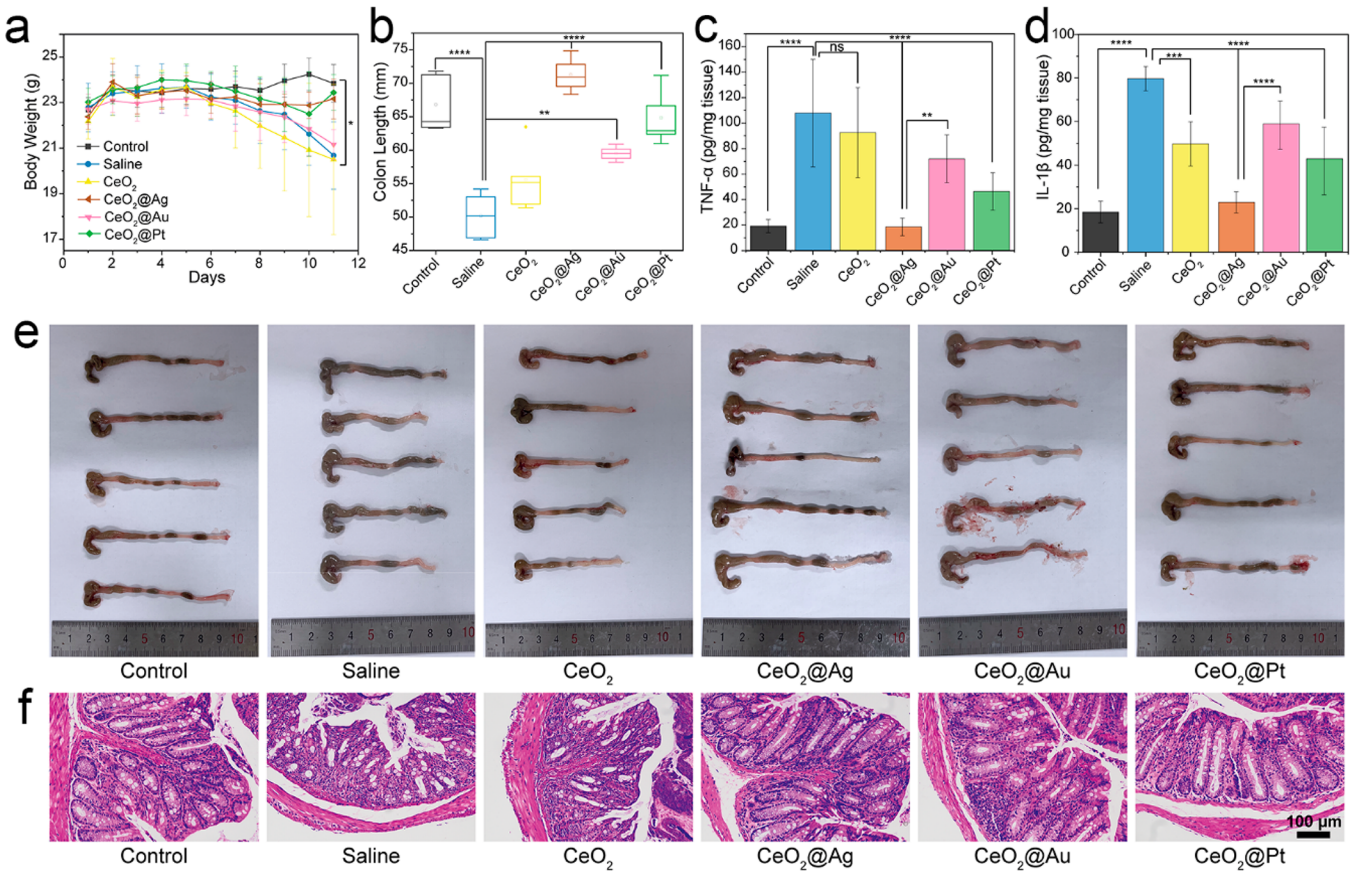

Figure 4. IBD therapy, tissue sections, and cytokine analysis. (a) Daily body weight recorded while undergoing treatments with different CeO_2@metal nanozymes. (b) Statistical length of colon taken on day 10. (c,d) IL-1β and TNF-α levels in colon homogenates after treatments. (e) Images of the colons taken on day 10. (f) H&E-stained images of colons following CeO_2@metal nanozymes treatment. The data are shown as means ± SD (n = 5). Analysis was performed using one-way ANOVA. Specific P-values are shown in the source data: *$P \leq 0.05$, **$P \leq 0.01$, ***$P \leq 0.001$, and ****$P \leq 0.0001$.

the XPS analysis corroborated this observation since a significant reduction in Ce^{3+} content (19.34%) and oxygen vacancies related peak (531.2 eV) was noticed, relative to hollow CeO_2 nanospheres (Figure S13). The exact content of different metals was determined by inductively coupled plasma optical emission spectrometry (ICP-OES), and the amounts of Ag, Au, and Pt were found to be around 105.0, 56.7, and 30.1 mg per gram of PVP capped hollow CeO_2 nanospheres, respectively.

ROS scavenging nanozymes hold great significance for a wide range of therapeutic applications; the scavenging capacities of CeO_2 and CeO_2@metal toward $O_2^{\bullet-}$ and H_2O_2 were determined. The SOD-like activity to eliminate $O_2^{\bullet-}$ was analyzed using a WST-1 kit. In the assay, the SOD-like activity of the different nanozymes was quantified by assessing the inhibition of formazan production (Figure S14a). CeO_2@Ag displayed the best SOD-like activity compared to the other two nanostructures (Figure S15). As catalase transforms lethal H_2O_2 into benign oxygen, the CAT-like activity of our nanostructures was determined by monitoring the decomposition of H_2O_2 using a dissolved oxygen meter. As presented in Figure S14b, CeO_2@Pt exhibited a superior CAT-like activity relative to the other two nanostructures. The activity of CeO_2@Ag was also appreciable enough to be considered as a CAT-like nanozyme. When compared with CeO_2 alone, both the SOD- and CAT-like activities of CeO_2@metal nanostructures were more superior and thus could be explored in inflammatory models. The biocompatibility of the CeO_2@metal nanozymes was evaluated in murine macrophages (RAW 264.7), which are often present in inflamed tissues, using the Cell Counting Kit-8 (CCK-8) assay. All compositions were found to be highly biocompatible and safe up to 25 μg/mL after 1 day of cocultivation (Figure S14c). To evaluate the cellular ROS scavenging activity, different CeO_2@metal nanostructures (10 μg/mL) were added to H_2O_2 (100 μM)-stimulated RAW 264.7 cells, and the fluorescence of 2,7-dichlorodihydrofluorescein diacetate (DCFH-DA, a fluorescence dye for intracellular ROS) was detected at an excitation wavelength of 488 nm. As shown in Figure S14d, in the presence of CeO_2@metal nanozymes, the fluorescence signal decreased ($P < 0.0003$) in CeO_2@Ag and CeO_2@Au, signifying the efficient ROS scavenging activity of nanozymes. Hollow CeO_2 also partially attenuated the fluorescent signals. These results suggest that the CeO_2@metal based nanozymes can scavenge ROS and protect cells from the ROS-induced oxidative damage. In an inflammatory condition, the expression of pro-inflammatory genes is markedly up-regulated in the macrophage cells, we performed qPCR analysis and expectedly found a significant upsurge ($P < 0.0001$) in IL-1β, TNF-α, and IL-6 mRNA expressions after inducing inflammation via LPS treatment in RAW 264.7 compared to control group (Figure S16). These elevated markers demonstrate the M1 polarization of macrophages. To evaluate the anti-inflammatory activities of our materials, RAW 264.7 cells

https://doi.org/10.1021/acsnano.2c07306
ACS Nano 2022, 16, 20567−20576

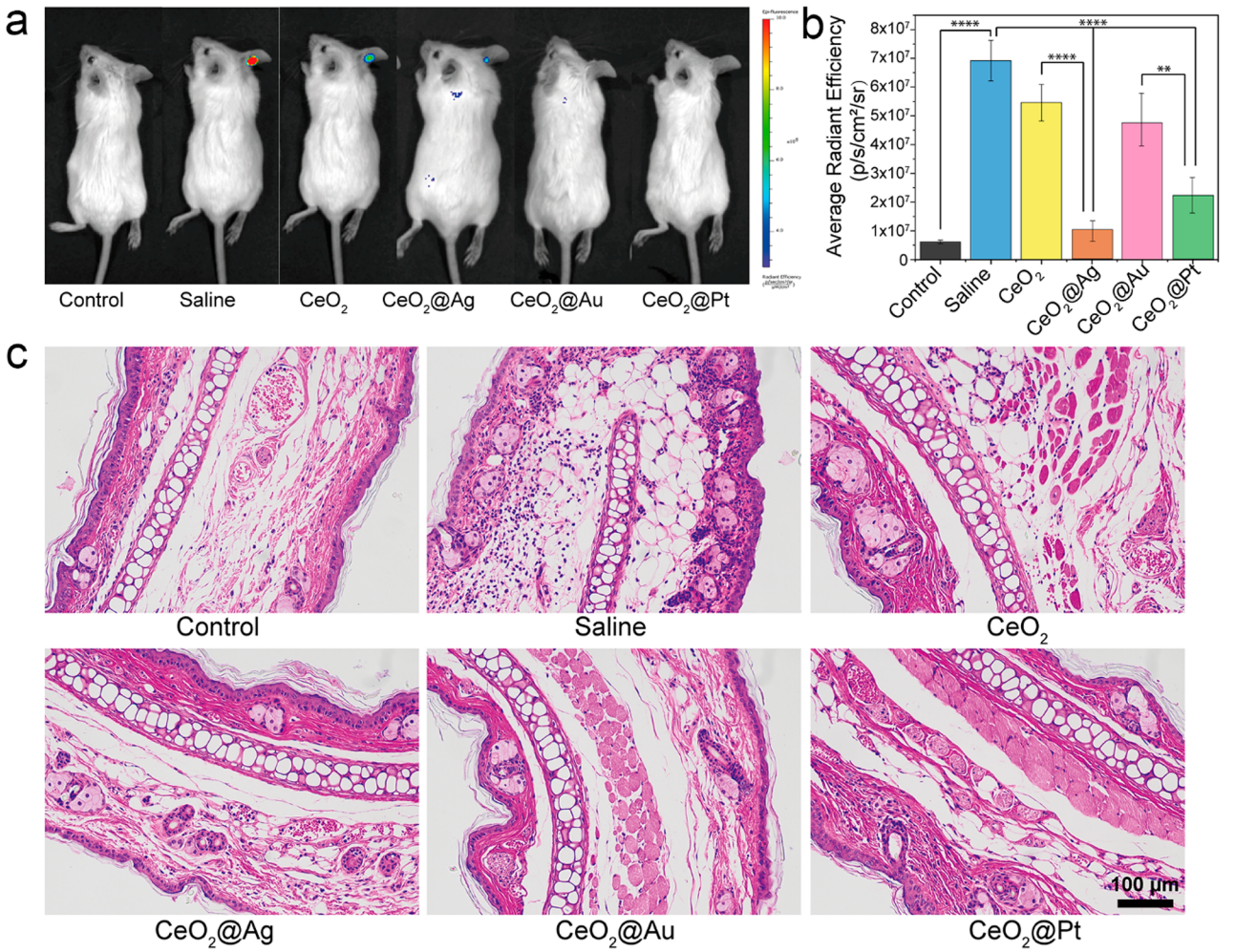

Figure 5. Anti-inflammatory activity in ear model. ***In vivo*** **fluorescence imaging of mice with PMA-induced ear inflammation after treatment with different CeO_2@metal nanozymes. (b) Total radiant efficiency of the fluorescence images acquired in live mice. (c) H&E-stained images of ear tissues after treatments with different CeO_2@metal nanozymes. The data are shown as means ± SD (n = 5). Analysis was performed using one-way ANOVA. Specific P-values are shown in the source data: *$P \leq 0.05$, **$P \leq 0.01$, ***$P \leq 0.001$, and ****$P \leq 0.0001$.**

were coincubated with LPS and CeO_2@metal nanozymes, a noticeable down regulation in pro-inflammatory cytokines was noticed, particularly CeO_2@Ag exhibited superior *in vitro* anti-inflammation efficacy ($P < 0.0001$) among the three CeO_2@metal nanozymes, showing the potential of these materials to be explored in animal models for effectively reducing the inflammation levels.

Encouraged by the biocompatibility, ROS scavenging capacities and anti-inflammatory characteristics, the *in vivo* therapeutic efficacy of CeO_2@metal nanozymes was investigated in a murine ulcerative colitis (UC) model.[62,63] To induce UC, dextran sulfate sodium (DSS) was first orally supplied (2 wt % aqueous solution) for six consecutive days (days 2 to 7) and subsequently a reduction in body weight ($P < 0.048$) indicated the successful onset of UC (Figure 4a). Different CeO_2@metal compositions were intraperitoneally injected as a therapy on three consecutive days (days 8, 9, and 10). The length of the colons in colitis-induced mice was found to be significantly shorter (50.19 ± 3.3 mm) than the length in normal mice (64.34 ± 4.04 mm). Therapeutic efficacy was then assessed by measuring the colon length variations and observing the pathological sections. CeO_2@Ag proved to be highly effective ($P < 0.0001$) for the recovery of colon parameters to normal levels at a concentration as low as 0.5 mg/kg, other CeO_2@metal nanozymes also displayed appreciable therapeutic activity ($P < 0.005$), as displayed in Figure 4b. A marked improvement in the histological appearance was expectedly observed in CeO_2@Ag and CeO_2@Pt treated groups comparable to normal mice, whereas a severe collapse in the epithelium and colonic tissues was noted in the DSS-induced colitis group, as shown in hematoxylin and eosin (H&E) stained colon sections (Figure 4f). ELISA assay was used to evaluated the levels of pro-inflammatory cytokines, the levels of both IL-1β and TNF-α were evidently increased in UC induced mice, whereas a significant downregulation was observed in CeO_2@metal treated groups, as shown in Figure 4c,d. The silver NPs containing composition exerted the maximum anti-inflammatory activity ($P < 0.0001$). Accumulation of nanozymes at the inflamed mucosa is a prerequisite for effective therapy against IBD, and at the same time the biodistribution of materials in other vital organs need to be taken into consideration to avoid acute toxicity. Therefore, we evaluated the biodistribution of CeO_2 and CeO_2@Ag in terms of cerium content using ICP-OES analysis. Following the intraperitoneal administration of CeO_2 and CeO_2@Ag nanozymes, mice were sacrificed and

https://doi.org/10.1021/acsnano.2c07306
ACS Nano 2022, 16, 20567−20576

their blood, urine, feces, heart, liver, spleen, lung, kidney, and colon were collected at different time scale (12, 24, 48, and 72 h). The highest accumulation was observed in colon and liver, and data indicated that the nanozymes were not inclined to accumulate in other vital organs (heart, lung, spleen, and kidney) and neither to be excreted through urine, revealing the efficacy and biosafety of the tested materials. Figure S17 indicates that the nanozymes uptaken by liver were also excreted (most likely into feces) within 72 h.

Normal tissues contain adequate amounts of protective enzymatic (such as SOD, catalase, and GSH peroxidase) and nonenzymatic antioxidants (such as thiols, ascorbate, and α-tocopherol) to scavenge damaging oxidizing agents (i.e., superoxide, hydrogen peroxide, hydroxyl radical, and hypochlorite). It is reported that a dysregulated immune system initiates the pathogenesis of IBD, and the resulting inflamed tissues produce an excessive amount of reactive oxygen and nitrogen species. Earlier reports demonstrated that high doses of antioxidants such as ascorbic acid and/or α-tocopherol could ameliorate the acute flares of disease and attenuate the inflammation associated with UC. Hence, it can be reasonably inferred that the enhanced anti-inflammatory therapeutic activity of CeO_2@metal nanozymes could be linked to their excellent ROS scavenging properties. In addition to antioxidant properties, the superior therapeutic activity of CeO_2@Ag can also be ascribed to the antibacterial activity of silver NPs. In previous reports, enhanced wound healing has been reported with topical application of Ag NPs.[64−66]

In addition to IBD therapy, the anti-inflammatory activity of CeO_2@metal nanozymes was also tested in an ear inflammation model, inflammation was induced by phorbol 12-myristate 13-acetate (PMA), as indicated in Figure S18. Following the samples administration, the variation in the fluorescence intensity of DCFH-DA indicated the ROS scavenging property, a pronounced reduction in fluorescence intensity following the CeO_2@metal treatment corroborates the *in vivo* ROS scavenging/anti-inflammatory activities (Figure 5a,b). Expectedly, both silver and platinum based nanozymes exhibited the best ROS scavenging activities ($P < 0.0001$), as was shown in the IBD model. Histopathological evaluation also verified that the groups with CeO_2@metal nanozymes had the lowest level of inflammation, while an obvious lymphocyte infiltration was observed in hematoxylin and eosin (H&E) stained images of PMA induced inflammatory model, as shown in Figure 5c. The *in vivo* toxicity of CeO_2 compositions to the main organs (heart, lungs, liver, spleen, and kidney) was assessed through histopathological observations, none of the experimental groups revealed noticeable toxicity (Figure S19). Taken together, our results reveal that CeO_2 based nanozymes possess superior ROS scavenging activities in inflammatory diseases.

CONCLUSION

In contrast to conventional approaches, we developed a straightforward method for the spontaneous deposition of multiple metallic NPs (Ag, Au, and Pt) onto the surface of redox active hollow CeO_2 nanospheres without using any pretreatment or additional reducing and stabilizing agents. Based on the composition of the resulting materials, we exploited their biocatalytic behavior in two *in vivo* inflammatory models. The multienzyme activities (SOD- and CAT-like) of the materials were translated well into *in vivo* models with successful treatment of UC and ear inflammation. The silver-containing composition showed superior therapeutic performance at a dose of 0.5 mg/kg. As the oxide-supported metals have garnered continuous attention due to their multifunctional and greatly enhanced properties that are difficult or even impossible to achieve in single metal NPs; hence, our simple oxygen vacancy-mediated metal growth strategy provides a direction for future research efforts to produce identical oxide supported nanocomposites for wide-ranging technological applications.

ASSOCIATED CONTENT

Supporting Information

The Supporting Information is available free of charge at https://pubs.acs.org/doi/10.1021/acsnano.2c07306.

Experimental section including materials synthesis, *in vitro* and *in vivo* procedures; effect of temperature, pH, and the presence of oxygen vacancies on metal NPs growth; HAADF-STEM images of CeO_2 substrates and their metal based compositions; XPS analysis of different CeO_2 substrates and respective metal based compositions; zeta potential measurement to demonstrate the adsorptions of metal precursors; ROS scavenging, *in vitro* anti-inflammatory, biodistribution, and biotoxicity data (PDF)

AUTHOR INFORMATION

Corresponding Author

Hui Wei − *College of Engineering and Applied Sciences, Nanjing National Laboratory of Microstructures, Jiangsu Key Laboratory of Artificial Functional Materials and State Key Laboratory of Analytical Chemistry for Life Science, School of Chemistry and Chemical Engineering, Chemistry and Biomedicine Innovation Center (ChemBIC), Nanjing University, Nanjing, Jiangsu 210023, China;* orcid.org/0000-0003-0870-7142; Email: weihui@nju.edu.cn

Authors

Faheem Muhammad − *College of Engineering and Applied Sciences, Nanjing National Laboratory of Microstructures, Jiangsu Key Laboratory of Artificial Functional Materials, Nanjing University, Nanjing, Jiangsu 210023, China*

Futao Huang − *College of Engineering and Applied Sciences, Nanjing National Laboratory of Microstructures, Jiangsu Key Laboratory of Artificial Functional Materials, Nanjing University, Nanjing, Jiangsu 210023, China*

Yuan Cheng − *College of Engineering and Applied Sciences, Nanjing National Laboratory of Microstructures, Jiangsu Key Laboratory of Artificial Functional Materials, Nanjing University, Nanjing, Jiangsu 210023, China*

Xiwen Chen − *College of Engineering and Applied Sciences, Nanjing National Laboratory of Microstructures, Jiangsu Key Laboratory of Artificial Functional Materials, Nanjing University, Nanjing, Jiangsu 210023, China*

Quan Wang − *College of Engineering and Applied Sciences, Nanjing National Laboratory of Microstructures, Jiangsu Key Laboratory of Artificial Functional Materials, Nanjing University, Nanjing, Jiangsu 210023, China*

Chenxin Zhu − *College of Engineering and Applied Sciences, Nanjing National Laboratory of Microstructures, Jiangsu Key Laboratory of Artificial Functional Materials, Nanjing University, Nanjing, Jiangsu 210023, China*

Yihong Zhang − *College of Engineering and Applied Sciences, Nanjing National Laboratory of Microstructures, Jiangsu Key Laboratory of Artificial Functional Materials, Nanjing University, Nanjing, Jiangsu 210023, China*
Xiaohan Yang − *State Key Laboratory of Pollution Control and Resource Reuse, School of Environment, Nanjing University, Nanjing, Jiangsu 210023, China*
Peng Wang − *College of Engineering and Applied Sciences, Nanjing National Laboratory of Microstructures, Jiangsu Key Laboratory of Artificial Functional Materials, Nanjing University, Nanjing, Jiangsu 210023, China;* orcid.org/0000-0003-0788-6687

Complete contact information is available at: https://pubs.acs.org/10.1021/acsnano.2c07306

Author Contributions

†F.M., F.H., and Y. C. contributed equally to this work.

Notes

The authors declare no competing financial interest.

ACKNOWLEDGMENTS

This work was supported by the National Key R&D Program of China (2021YFF1200700 and 2019YFA0709200), National Natural Science Foundation of China (21874067, 21722503, and 11874199), PAPD Program, and Fundamental Research Funds for the Central Universities (021314380195) and Jiangsu Provincial Key R&D Program (BE2022836). We are highly thankful to Professor Guandao Gao for providing access to the ICP-OES instrument.

REFERENCES

(1) Bing, Y.; Liu, H.; Zhang, L.; Ghosh, D.; Zhang, J. Nanostructured Pt-Alloy Electrocatalysts for PEM Fuel Cell Oxygen Reduction Reaction. *Chem. Soc. Rev.* **2010**, *39*, 2184−2202.
(2) Gellé, A.; Jin, T.; de la Garza, L.; Price, G. D.; Besteiro, L. V.; Moores, A. Applications of Plasmon-Enhanced Nanocatalysis to Organic Transformations. *Chem. Rev.* **2020**, *120*, 986−1041.
(3) Ishida, T.; Murayama, T.; Taketoshi, A.; Haruta, M. Importance of Size and Contact Structure of Gold Nanoparticles for the Genesis of Unique Catalytic Processes. *Chem. Rev.* **2020**, *120*, 464−525.
(4) Personick, M. L.; Madix, R. J.; Friend, C. M. Selective Oxygen-Assisted Reactions of Alcohols and Amines Catalyzed by Metallic Gold: Paradigms for the Design of Catalytic Processes. *ACS Catal.* **2017**, *7*, 965−985.
(5) Wang, X.; Song, S.; Zhang, H. A Redox Interaction-Engaged Strategy for Multicomponent Nanomaterials. *Chem. Soc. Rev.* **2020**, *49*, 736−764.
(6) Dimitratos, N.; Lopez-Sanchez, J. A.; Hutchings, G. J. Selective Liquid Phase Oxidation with Supported Metal Nanoparticles. *Chem. Sci.* **2012**, *3*, 20−44.
(7) Mulvaney, P.; Giersig, M.; Ung, T.; Liz-Marzán, L. M. Direct Observation of Chemical Reactions in Silica-Coated Gold and Silver Nanoparticles. *Adv. Mater.* **1997**, *9*, 570−575.
(8) Baroliya, P. K.; Chopra, J.; Pal, T.; Maiti, S.; Al-Thabaiti, S. A.; Mokhtar, M.; Maiti, D. Supported Metal Nanoparticles Assisted Catalysis: A Broad Concept in Functionalization of Ubiquitous C−H Bonds. *ChemCatChem.* **2021**, *13*, 4655−4678.
(9) Abad, A.; Concepción, P.; Corma, A.; García, H. A Collaborative Effect between Gold and a Support Induces the Selective Oxidation of Alcohols. *Angew. Chem., Int. Ed.* **2005**, *44*, 4066−4069.
(10) Barakat, T.; Rooke, J. C.; Tidahy, H. L.; Hosseini, M.; Cousin, R.; Lamonier, J.-F.; Giraudon, J.-M.; De Weireld, G.; Su, B.-L.; Siffert, S. Noble-Metal-Based Catalysts Supported on Zeolites and Macro-Mesoporous Metal Oxide Supports for the Total Oxidation of Volatile Organic Compounds. *ChemSusChem* **2011**, *4*, 1420−1430.
(11) Enache, D. I.; Edwards, J. K.; Landon, P.; Solsona-Espriu, B.; Carley, A. F.; Herzing, A. A.; Watanabe, M.; Kiely, C. J.; Knight, D. W.; Hutchings, G. J. Solvent-Free Oxidation of Primary Alcohols to Aldehydes Using Au-Pd/-TiO_2 Catalysts. *Science* **2006**, *311*, 362−365.
(12) Liu, G.; Wang, D.; Zhou, F.; Liu, W. Electrostatic Self-Assembly of Au Nanoparticles onto Thermosensitive Magnetic Core-Shell Microgels for Thermally Tunable and Magnetically Recyclable Catalysis. *Small* **2015**, *11*, 2807−2816.
(13) Heckert, E. G.; Karakoti, A. S.; Seal, S.; Self, W. T. The Role of Cerium Redox State in the SOD Mimetic Activity of Nanoceria. *Biomaterials* **2008**, *29*, 2705−2709.
(14) Haruta, M.; Tsubota, S.; Kobayashi, T.; Kageyama, H.; Genet, M. J.; Delmon, B. Low-Temperature Oxidation of Co over Gold Supported on TiO_2, α–Fe_2O_3, and Co_3O_4. *J. Catal.* **1993**, *144*, 175−192.
(15) Shiraishi, Y.; Sakamoto, H.; Sugano, Y.; Ichikawa, S.; Hirai, T. Pt−Cu Bimetallic Alloy Nanoparticles Supported on Anatase TiO_2: Highly Active Catalysts for Aerobic Oxidation Driven by Visible Light. *ACS Nano* **2013**, *7*, 9287−9297.
(16) Wang, J.; Gu, X.; Pei, L.; Kong, P.; Zhang, J.; Wang, X.; Wang, R.; Waclawik, E. R.; Zheng, Z. Strong Metal-Support Interaction Induced O_2 Activation over Au/MNb_2O_6 (M = Zn^{2+}, Ni^{2+} and Co^{2+}) for Efficient Photocatalytic Benzyl Alcohol Oxidative Esterification. *Appl. Catal., B* **2021**, *283*, 119618.
(17) Shiraishi, Y.; Toi, S.; Ichikawa, S.; Hirai, T. Photocatalytic NH_3 Splitting on TiO_2 Particles Decorated with Pt−Au Bimetallic Alloy Nanoparticles. *ACS Appl. Nano Mater.* **2020**, *3*, 1612−1620.
(18) Akashi, R.; Naya, S.-i.; Negishi, R.; Tada, H. Two-Step Excitation-Driven Au−TiO_2−CuO Three-Component Plasmonic Photocatalyst: Selective Aerobic Oxidation of Cyclohexylamine to Cyclohexanone. *J. Phys. Chem. C* **2016**, *120*, 27989−27995.
(19) Trogadas, P.; Fuller, T. F.; Strasser, P. Carbon as Catalyst and Support for Electrochemical Energy Conversion. *Carbon* **2014**, *75*, 5−42.
(20) Silbaugh, T. L.; Devlaminck, P.; Sofranko, J. A.; Barteau, M. A. Selective Oxidation of Ethanol over Ag, Cu and Au Nanoparticles Supported on Li_2O/ γ-Al_2O_3. *J. Catal.* **2018**, *364*, 40−47.
(21) Mahdavi-Shakib, A.; Sempel, J.; Hoffman, M.; Oza, A.; Bennett, E.; Owen, J. S.; Rahmani Chokanlu, A.; Frederick, B. G.; Austin, R. N. Au/TiO_2-Catalyzed Benzyl Alcohol Oxidation on Morphologically Precise Anatase Nanoparticles. *ACS Appl. Mater. Interfaces* **2021**, *13*, 11793−11804.
(22) Hu, Y.; Jensen, J. O.; Cleemann, L. N.; Brandes, B. A.; Li, Q. Synthesis of Pt−Rare Earth Metal Nanoalloys. *J. Am. Chem. Soc.* **2020**, *142*, 953−961.
(23) McDarby, S. P.; Wang, C. J.; King, M. E.; Personick, M. L. An Integrated Electrochemistry Approach to the Design and Synthesis of Polyhedral Noble Metal Nanoparticles. *J. Am. Chem. Soc.* **2020**, *142*, 21322−21335.
(24) Yu, Y.; Yang, W.; Sun, X.; Zhu, W.; Li, X. Z.; Sellmyer, D. J.; Sun, S. Monodisperse MPt (M = Fe, Co, Ni, Cu, Zn) Nanoparticles Prepared from a Facile Oleylamine Reduction of Metal Salts. *Nano Lett.* **2014**, *14*, 2778−2782.
(25) Cueto, M.; Sanz, M.; Oujja, M.; Gámez, F.; Martínez-Haya, B.; Castillejo, M. Platinum Nanoparticles Prepared by Laser Ablation in Aqueous Solutions: Fabrication and Application to Laser Desorption Ionization. *J. Phys. Chem. C* **2011**, *115*, 22217−22224.
(26) Hayden, B. E.; Pletcher, D.; Suchsland, J.-P.; Williams, L. J. The Influence of Pt Particle Size on the Surface Oxidation of Titania Supported Platinum. *Phys. Chem. Chem. Phys.* **2009**, *11*, 1564−1570.
(27) Saedy, S.; Palagin, D.; Safonova, O.; van Bokhoven, J. A.; Khodadadi, A. A.; Mortazavi, Y. Understanding the Mechanism of Synthesis of Pt_3Co Intermetallic Nanoparticles Via Preferential Chemical Vapor Deposition. *J. Mater. Chem. A* **2017**, *5*, 24396−24406.
(28) Park, J.; An, K.; Hwang, Y.; Park, J.-G.; Noh, H.-J.; Kim, J.-Y.; Park, J.-H.; Hwang, N.-M.; Hyeon, T. Ultra-Large-Scale Syntheses of Monodisperse Nanocrystals. *Nat. Mater.* **2004**, *3*, 891−895.

(29) Zakhtser, A.; Naitabdi, A.; Benbalagh, R.; Rochet, F.; Salzemann, C.; Petit, C.; Giorgio, S. Chemical Evolution of Pt−Zn Nanoalloys Dressed in Oleylamine. *ACS Nano* **2021**, *15*, 4018−4033.
(30) Carbone, L.; Cozzoli, P. D. Colloidal Heterostructured Nanocrystals: Synthesis and Growth Mechanisms. *Nano Today* **2010**, *5*, 449−493.
(31) Wuithschick, M.; Witte, S.; Kettemann, F.; Rademann, K.; Polte, J. Illustrating the Formation of Metal Nanoparticles with a Growth Concept Based on Colloidal Stability. *Phys. Chem. Chem. Phys.* **2015**, *17*, 19895−19900.
(32) Oh, M. H.; Yu, T.; Yu, S.-H.; Lim, B.; Ko, K.-T.; Willinger, M.-G.; Seo, D.-H.; Kim, B. H.; Cho, M. G.; Park, J.-H.; Kang, K.; Sung, Y.-E.; Pinna, N.; Hyeon, T. Galvanic Replacement Reactions in Metal Oxide Nanocrystals. *Science* **2013**, *340*, 964−968.
(33) Wang, X.; Zhang, Y.; Song, S.; Yang, X.; Wang, Z.; Jin, R.; Zhang, H. L-Arginine-Triggered Self-Assembly of CeO_2 Nanosheaths on Palladium Nanoparticles in Water. *Angew. Chem., Int. Ed.* **2016**, *55*, 4542−4546.
(34) Li, L.; Liu, Y.; Wang, Q.; Zhou, X.; Li, J.; Song, S.; Zhang, H. CeO_2 Supported Low-Loading Au as an Enhanced Catalyst for Low Temperature Oxidation of Carbon Monoxide. *CrystEngComm* **2019**, *21*, 7108−7113.
(35) Kim, K. W.; Kim, S. M.; Choi, S.; Kim, J.; Lee, I. S. Electroless Pt Deposition on Mn_3O_4 Nanoparticles Via the Galvanic Replacement Process: Electrocatalytic Nanocomposite with Enhanced Performance for Oxygen Reduction Reaction. *ACS Nano* **2012**, *6*, 5122−5129.
(36) Kim, S. M.; Jeon, M.; Kim, K. W.; Park, J.; Lee, I. S. Postsynthetic Functionalization of a Hollow Silica Nanoreactor with Manganese Oxide-Immobilized Metal Nanocrystals inside the Cavity. *J. Am. Chem. Soc.* **2013**, *135*, 15714−15717.
(37) Xi, G.; Ye, J.; Ma, Q.; Su, N.; Bai, H.; Wang, C. In Situ Growth of Metal Particles on 3d Urchin-Like WO_3 Nanostructures. *J. Am. Chem. Soc.* **2012**, *134*, 6508−6511.
(38) Zhu, Y.; Zhang, X.; Koh, K.; Kovarik, L.; Fulton, J. L.; Rosso, K. M.; Gutiérrez, O. Y. Inverse Iron Oxide/Metal Catalysts from Galvanic Replacement. *Nat. Commun.* **2020**, *11*, 3269.
(39) Pan, X.; Xu, Y.-J. Efficient Thermal- and Photocatalyst of Pd Nanoparticles on TiO_2 Achieved by an Oxygen Vacancies Promoted Synthesis Strategy. *ACS Appl. Mater. Interfaces* **2014**, *6*, 1879−1886.
(40) Kayama, T.; Yamazaki, K.; Shinjoh, H. Nanostructured Ceria−Silver Synthesized in a One-Pot Redox Reaction Catalyzes Carbon Oxidation. *J. Am. Chem. Soc.* **2010**, *132*, 13154−13155.
(41) Mitsudome, T.; Yamamoto, M.; Maeno, Z.; Mizugaki, T.; Jitsukawa, K.; Kaneda, K. One-Step Synthesis of Core-Gold/Shell-Ceria Nanomaterial and Its Catalysis for Highly Selective Semihydrogenation of Alkynes. *J. Am. Chem. Soc.* **2015**, *137*, 13452−13455.
(42) Wang, X.; Liu, D.; Li, J.; Zhen, J.; Wang, F.; Zhang, H. γ-Al_2O_3 Supported Pd@CeO_2 Core@Shell Nanospheres: Salting-out Assisted Growth and Self-Assembly, and Their Catalytic Performance in Co Oxidation. *Chem. Sci.* **2015**, *6*, 2877−2884.
(43) Wang, X.; Liu, D.; Song, S.; Zhang, H. CeO2@Pt Multicore@Shell Self-Assembled Nanospheres: Clean Synthesis, Structure Optimization, and Catalytic Applications. *J. Am. Chem. Soc.* **2013**, *135*, 15864−15872.
(44) Wei, H.; Wang, E. Nanomaterials with Enzyme-Like Characteristics (Nanozymes): Next-Generation Artificial Enzymes. *Chem. Soc. Rev.* **2013**, *42*, 6060−6093.
(45) Lin, A.; Sun, Z.; Xu, X.; Zhao, S.; Li, J.; Sun, H.; Wang, Q.; Jiang, Q.; Wei, H.; Shi, D. Self-Cascade Uricase/Catalase Mimics Alleviate Acute Gout. *Nano Lett.* **2022**, *22*, 508−516.
(46) Huang, L.; Chen, J.; Gan, L.; Wang, J.; Dong, S. Single-Atom Nanozymes. *Sci. Adv.* **2019**, *5*, eaav5490.
(47) Gao, L.; Zhuang, J.; Nie, L.; Zhang, J.; Zhang, Y.; Gu, N.; Wang, T.; Feng, J.; Yang, D.; Perrett, S.; Yan, X. Intrinsic Peroxidase-Like Activity of Ferromagnetic Nanoparticles. *Nat. Nanotechnol.* **2007**, *2*, 577−583.
(48) Zhang, X.; Liu, Y.; Gopalakrishnan, S.; Castellanos-Garcia, L.; Li, G.; Malassiné, M.; Uddin, I.; Huang, R.; Luther, D. C.; Vachet, R. W.; Rotello, V. M. Intracellular Activation of Bioorthogonal Nanozymes through Endosomal Proteolysis of the Protein Corona. *ACS Nano* **2020**, *14*, 4767−4773.
(49) Mu, J.; He, L.; Fan, W.; Tang, W.; Wang, Z.; Jiang, C.; Zhang, D.; Liu, Y.; Deng, H.; Zou, J.; Jacobson, O.; Qu, J.; Huang, P.; Chen, X. Cascade Reactions Catalyzed by Planar Metal−Organic Framework Hybrid Architecture for Combined Cancer Therapy. *Small* **2020**, *16*, 2004016.
(50) Zandieh, M.; Liu, J. Nanozyme Catalytic Turnover and Self-Limited Reactions. *ACS Nano* **2021**, *15*, 15645−15655.
(51) Zhu, P.; Chen, Y.; Shi, J. Nanoenzyme-Augmented Cancer Sonodynamic Therapy by Catalytic Tumor Oxygenation. *ACS Nano* **2018**, *12*, 3780−3795.
(52) Han, S. I.; Lee, S.-w.; Cho, M. G.; Yoo, J. M.; Oh, M. H.; Jeong, B.; Kim, D.; Park, O. K.; Kim, J.; Namkoong, E.; Jo, J.; Lee, N.; Lim, C.; Soh, M.; Sung, Y.-E.; Yoo, J.; Park, K.; Hyeon, T. Epitaxially Strained CeO_2/Mn_3O_4 Nanocrystals as an Enhanced Antioxidant for Radioprotection. *Adv. Mater.* **2020**, *32*, 2001566.
(53) Huang, R.; Li, C.-H.; Cao-Milán, R.; He, L. D.; Makabenta, J. M.; Zhang, X.; Yu, E.; Rotello, V. M. Polymer-Based Bioorthogonal Nanocatalysts for the Treatment of Bacterial Biofilms. *J. Am. Chem. Soc.* **2020**, *142*, 10723−10729.
(54) Vernekar, A. A.; Sinha, D.; Srivastava, S.; Paramasivam, P. U.; D'Silva, P.; Mugesh, G. An Antioxidant Nanozyme That Uncovers the Cytoprotective Potential of Vanadia Nanowires. *Nat. Commun.* **2014**, *5*, 5301.
(55) Kwon, H. J.; Kim, D.; Seo, K.; Kim, Y. G.; Han, S. I.; Kang, T.; Soh, M.; Hyeon, T. Ceria Nanoparticle Systems for Selective Scavenging of Mitochondrial, Intracellular, and Extracellular Reactive Oxygen Species in Parkinson's Disease. *Angew. Chem., Int. Ed.* **2018**, *57*, 9408−9412.
(56) Dong, H.; Fan, Y.; Zhang, W.; Gu, N.; Zhang, Y. Catalytic Mechanisms of Nanozymes and Their Applications in Biomedicine. *Bioconjugate Chem.* **2019**, *30*, 1273−1296.
(57) Pan, X.; Xu, Y.-J. Defect-Mediated Growth of Noble-Metal (Ag, Pt, and Pd) Nanoparticles on TiO_2 with Oxygen Vacancies for Photocatalytic Redox Reactions under Visible Light. *J. Phys. Chem. C* **2013**, *117*, 17996−18005.
(58) Wang, G.; Yang, Y.; Han, D.; Li, Y. Oxygen Defective Metal Oxides for Energy Conversion and Storage. *Nano Today* **2017**, *13*, 23−39.
(59) Liu, W.; Deng, T.; Feng, L.; Xie, A.; Zhang, J.; Wang, S.; Liu, X.; Yang, Y.; Guo, J. Designed Synthesis and Formation Mechanism of CeO_2 Hollow Nanospheres and Their Facile Functionalization with Au Nanoparticles. *CrystEngComm* **2015**, *17*, 4850−4858.
(60) Kumar, A.; Babu, S.; Karakoti, A. S.; Schulte, A.; Seal, S. Luminescence Properties of Europium-Doped Cerium Oxide Nanoparticles: Role of Vacancy and Oxidation States. *Langmuir* **2009**, *25*, 10998−11007.
(61) Jampaiah, D.; Ippolito, S. J.; Sabri, Y. M.; Reddy, B. M.; Bhargava, S. K. Highly Efficient Nanosized Mn and Fe Codoped Ceria-Based Solid Solutions for Elemental Mercury Removal at Low Flue Gas Temperatures. *Catal. Sci. Technol.* **2015**, *5*, 2913−2924.
(62) Liu, Y.; Cheng, Y.; Zhang, H.; Zhou, M.; Yu, Y.; Lin, S.; Jiang, B.; Zhao, X.; Miao, L.; Wei, C.-W.; Liu, Q.; Lin, Y.-W.; Du, Y.; Butch, C. J.; Wei, H. Integrated Cascade Nanozyme Catalyzes in Vivo Ros Scavenging for Anti-Inflammatory Therapy. *Sci. Adv.* **2020**, *6*, eabb2695.
(63) Wu, J.; Yu, Y.; Cheng, Y.; Cheng, C.; Zhang, Y.; Jiang, B.; Zhao, X.; Miao, L.; Wei, H. Ligand-Dependent Activity Engineering of Glutathione Peroxidase-Mimicking Mil-47(V) Metal−Organic Framework Nanozyme for Therapy. *Angew. Chem., Int. Ed.* **2021**, *60*, 1227−1234.
(64) Dunn, K.; Edwards-Jones, V. The Role of Acticoat with Nanocrystalline Silver in the Management of Burns. *Burns* **2004**, *30*, S1−S9.

https://doi.org/10.1021/acsnano.2c07306
ACS Nano 2022, 16, 20567−20576

(65) Chen, H.; Cheng, R.; Zhao, X.; Zhang, Y.; Tam, A.; Yan, Y.; Shen, H.; Zhang, Y. S.; Qi, J.; Feng, Y.; Liu, L.; Pan, G.; Cui, W.; Deng, L. An Injectable Self-Healing Coordinative Hydrogel with Antibacterial and Angiogenic Properties for Diabetic Skin Wound Repair. *NPG Asia Mater.* **2019**, *11*, 3.
(66) Tian, J.; Wong, K. K. Y.; Ho, C.-M.; Lok, C.-N.; Yu, W.-Y.; Che, C.-M.; Chiu, J.-F.; Tam, P. K. H. Topical Delivery of Silver Nanoparticles Promotes Wound Healing. *ChemMedChem.* **2007**, *2*, 129−136.

https://doi.org/10.1021/acsnano.2c07306
ACS Nano 2022, 16, 20567−20576